Chemical Science

EDGE ARTICLE

View Article Online
View Journal | View Issue

Cite this: *Chem. Sci.*, 2017, **8**, 7954

The significance of bromide in the Brust–Schiffrin synthesis of thiol protected gold nanoparticles†

S. G. Booth,[a] A. Uehara,[*b] S.-Y. Chang,[c] C. La Fontaine,[d] T. Fujii,[e] Y. Okamoto,[f] T. Imai,[g] S. L. M. Schroeder[ch] and R. A. W. Dryfe[*a]

Received 27th July 2017
Accepted 26th September 2017

DOI: 10.1039/c7sc03266h

rsc.li/chemical-science

The mechanism of the two-phase Brust–Schiffrin synthesis of alkane thiol protected metal nanoparticles is known to be highly sensitive to the precursor species and reactant conditions. In this work X-ray absorption spectroscopy is used in conjunction with liquid/liquid electrochemistry to highlight the significance of Br^- in the reaction mechanism. The species $[AuBr_4]^-$ is shown to be a preferable precursor in the Brust–Schiffrin method as it is more resistant to the formation of Au(I) thiolate species than $[AuCl_4]^-$. Previous literature has demonstrated that avoidance of the Au(I) thiolate is critical to achieving a good yield of nanoparticles, as $[Au(I)X_2]^-$ species are more readily reduced by $NaBH_4$. We propose that the observed behavior of $[AuBr_4]^-$ species described herein explains the discrepancies in reported behavior present in the literature to date. This new mechanistic understanding should enable nanoparticle synthesis with a higher yield and reduce particle size polydispersity.

Introduction

There have been numerous publications on the synthesis, stabilisation and manipulation of metal nanoparticles in order to exploit their size-tuneable properties. These open up the prospect of applications including therapeutics, catalysis and plasmonic devices. Due to the stability of the material, gold nanoparticles have drawn the most interest. Whilst numerous synthetic procedures exist, the two most significant methods to produce spherical particles are those of Turkevich and Frens,[1,2] to produce citrate protected particles in an aqueous suspension, and Brust, Schiffrin and co-workers,[3,4] to produce thiol protected particles stable in an organic suspension.

The publication by Brust *et al.*, describing a simple 2-phase reaction to produce alkane thiol coated nanoparticles was a landmark in the field of metal nanoparticle synthesis.[3,5] The method produces spherical Au nanoparticles where the mean particle diameter can be tailored across the range 1–6 nm by varying the thiol : Au ratio. The particles have a very uniform size distribution and can be dried and re-suspended in numerous organic solvents without aggregation. The initial method has been further refined to produce a single phase approach, extended to various metals (including Ag, Cu and Pd), and modified through post-synthetic methods to exchange the surface ligands on the nanoparticles, or refine the dispersions to form metal clusters with a uniform composition.[4–12] Recently, the reaction mechanism has been a focus of research as it has been found to be significantly more complex than was initially suggested.[13] The net reaction involves the transfer of a Au(III) salt from water to toluene through the use of a phase transfer catalyst. This is followed by the removal of the initial aqueous solution. Subsequent addition of an alkane thiol and $NaBH_4$ then reduces the Au(III) species in the organic phase, resulting in the formation of thiol protected particles, Fig. 1.

However, further investigation has been required to understand the possible complications at each stage of the reaction. Mechanistic studies have now led to a consensus on the reactions involved in each step of the original synthesis. Initially TOA^+Br^- (tetraoctylammonium bromide), often written as TOAB, in toluene is brought into contact with the aqueous $[AuCl_4]^-$ solution to facilitate transfer into the organic phase. The use of TOA^+Br^- means that halide ion exchange is possible, leading to a mixed halide gold species, $[AuX_4]^-_{(org)}$, of unknown composition. (X represents either Cl^- or Br^- when the exact identity is unknown.)

As an alternative, TOA^+Cl^- (tetraoctylammonium chloride) may be used to avoid this halide exchange. The phase transfer

[a]School of Chemistry, University of Manchester, Manchester, M13 9PL, UK. E-mail: robert.dryfe@manchester.ac.uk
[b]Division of Nuclear Engineering Science, Research Reactor Institute, Kyoto University, Kumatori, Sennan, Osaka, 590-0494, Japan. E-mail: auehara@rri.kyoto-u.ac.jp
[c]Diamond Light Source Ltd., Didcot, Oxfordshire OX11 0DE, UK
[d]Synchrotron Soleil, L'Orme des Merisiers, Saint-Aubin, BP48, 91192, Gif-sur-Yvette, France
[e]Division of Sustainable Energy and Environmental Engineering, Graduate School of Engineering, Osaka University, Suita, Osaka, 565-0871, Japan
[f]Materials Sciences Research Center, Japan Atomic Energy Agency, 2-4, Shirakata, Tokai, Naka, Ibaraki, 319-1195, Japan
[g]Department of Materials Chemistry, Faculty of Science and Technology, Ryukoku University, Otsu, Shiga 520-2194, Japan
[h]School of Chemical and Process Engineering, University of Leeds, Leeds LS2 9JT, UK

† Electronic supplementary information (ESI) available. See DOI: 10.1039/c7sc03266h

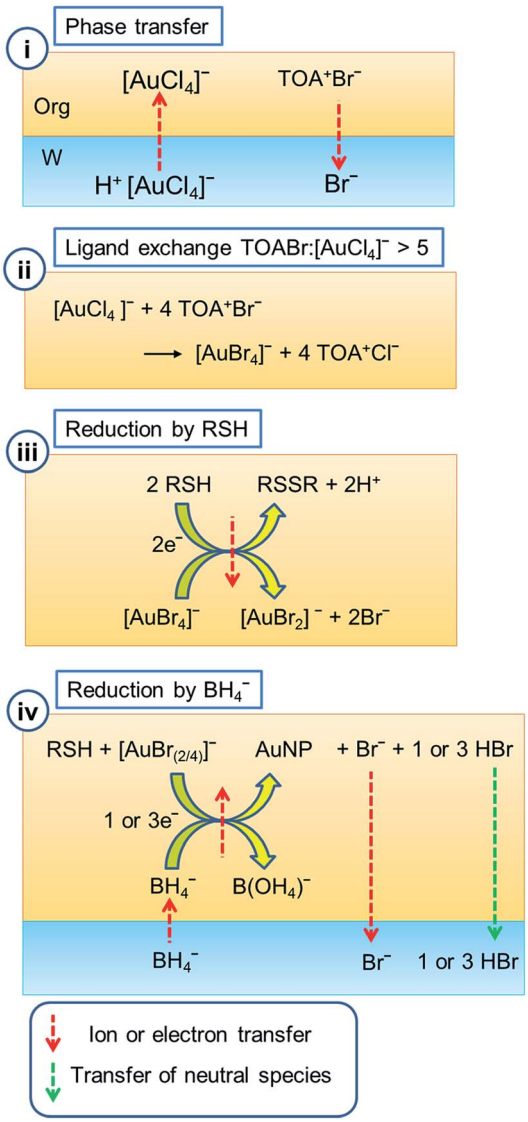

Fig. 1 Schematic illustration of the steps involved in the two phase synthesis method. In the illustration the aqueous phase is drawn as blue and the toluene phase as yellow. Step 1 is the Au phase transfer, step 2 shows the halide ion exchange process, step 3 shows the addition of alkane thiol causing a reduction to Au(I), and step 4 is the phase transfer process occurring on addition of $NaBH_4$ leading to nanoparticle formation.

has been shown to occur through an ion pair process[14,15] rather than the previously proposed reverse micelle formation.[16–21] The addition of alkane thiol, added as a capping agent, has been shown to cause the reduction of Au(III) to Au(I).[22] Preliminary studies initially assumed that the identity of the Au(I) species was a polymeric Au–SR species. This species is visible as a white precipitate at the liquid/liquid interface if the aqueous phase is retained. The important work of Goulet and Lennox disputed this and proposed that in the absence of water, the intermediate species was in fact $[AuX_2]^-$. This was the only intermediate species observed in their reaction.[13] Subsequent work has however shown that formation of Au(I)SR in a single phase is indeed possible, normally as a minor component.[23–25]

The Au-thiolate species form if (a) the aqueous phase is retained during the reaction; (b) at high reactant concentrations; and (c) at thiol : Au ratios greater than 2 : 1.[16,23,24] Whilst the soluble Au(I)SR species can be reduced by BH_4^- it appears that the insoluble polymeric species are not readily reduced, leading to greater polydispersity and a lower yield of the nanoparticles if the thiolate is formed.[25] Finally, when the organic AuX_2/Au(I)SR solution is brought into contact with aqueous $NaBH_4$, the BH_4^- ion is transferred to the organic phase by the excess TOA^+, added to transfer the $[AuCl_4]^-$ species from the aqueous to the organic phase.[25–27] Following BH_4^- phase transfer, the reduction of Au(I) to Au(0) by BH_4^- to form the metal nanoparticles occurs in the bulk organic phase.

A variety of techniques have been applied to discern the processes involved in the Brust–Schiffrin synthesis, which in combination have been able to draw out a thorough picture of the reaction. These include spectroscopy (NMR and Raman), DFT calculations, XAFS (X-ray absorption fine structure) and electrochemistry.[10,13,18,25,28,29] XAFS can provide clear information on the oxidation state (through the XANES – X-ray absorption near edge structure) and local bonding (through the EXAFS – extended X-ray absorption fine structure) around a target absorber. In the case of the Au L_3-edge, excitation of core 2p electrons into unoccupied 5d/6s orbitals takes place. The absorption coefficient for this process provides information about the local unoccupied density of states, which correlates with the oxidation state of the absorber. In addition, the XANES is also sensitive to multiple scattering of the excited photoelectron waves, leading to additional sensitivity to changes in oxidation state, local bonding and geometric conformation changes of the complex. An incisive understanding of the composition of samples can be achieved through linear combination fitting using standard reference spectra. The EXAFS can provide the local structure around the absorber through iterative curve fitting to a calculated EXAFS model. One of the complications that has limited the usefulness of EXAFS in regard to the Brust–Schiffrin synthesis is the similarity of the electron scattering cross sections of Cl and S. As the two elements are located side by side in the periodic table their atomic cores have the same number of electrons, leading to indistinguishable backscattering behavior in EXAFS when their bond lengths to the X-ray absorber are similar. Therefore, when examining mixed component systems, where the Cl/S ratio was not certain, it was not possible to separate the contributions of M–Cl and M–S scattering with certainty. However, when the heavier halide ion is substituted ($[AuBr_4]^-$ instead of $[AuCl_4]^-$), there is a clear variation in bond length and backscattering properties between M–Br and M–S, permitting more definitive examination of the chemical variations.

Electrochemistry at a liquid/liquid interface is likewise very sensitive to the structural composition of intermediate species, and thereby provides complementary information. As the Gibbs energy of transfer varies depending on the speciation of an ion it is possible to observe the different species and to measure relative concentrations through analysis of the current response. This method has been utilized in order to successfully follow a number of different deposition procedures.[30–35] A

micro-scale liquid/liquid interface is utilised in order to expand the potential window and minimise the influence of water on the system. It has recently been reported that toluene can be used as the organic phase in a micro-liquid/liquid system[36] therefore enabling us to confirm the relevance of the results to the original Brust–Schiffrin reaction.

In the following we will demonstrate that by examining the Au speciation during the reduction procedure by combined XAFS and liquid/liquid electrochemistry we can confirm the significance of Br^- in the reduction protocol suggested by Goulet and Lennox.[13] The measurements conducted using either TOA^+Br^- or TOA^+Cl^- as the phase transfer catalyst demonstrate that the reduction pathway is significantly influenced by the presence of Br^-.

Experimental

Chemicals

All reagents were used as purchased from the manufacturers without further purification. $HAuCl_4$ (99.99%) and $NaAuBr_4$ (99.99%) were purchased from Alfa-Aesar (Heysham, UK). Toluene (99.8%, anhydrous), ααα-trifluorotoluene (TFT, ≥99%, anhydrous), 1,2-dichloroethane (99.8%, anhydrous), tetraoctylammonium chloride (TOA^+Cl^-, ≥97%), tetraoctylammonium bromide (TOA^+Br^-, 98%), 1-dodecane thiol (≥98%) and sodium borohydride (≥98%) were purchased from Sigma-Aldrich (Dorset, UK). In order to form organic phase solutions of the metal salts, 10 mM aqueous solutions were brought into contact with the organic TFT phase containing TOA^+Cl^- for the chloride complexes, or TOA^+Br^- for the bromide complexes, to avoid the formation of mixed halide species, and shaken to induce phase transfer. Further details were described in ref 25. All glassware was cleaned with Piranha (H_2O_2/H_2SO_4 – CAUTION, handle with care) solution prior to use. Ultrapure water (Milli-q, 18.2 MΩ cm) was used to prepare all aqueous solutions.

XAFS measurements

Measurements were conducted on the quick EXAFS (QEXAFS) beamline ROCK[37] at the Synchrotron SOLEIL facility (Saint Aubin, France) and EXAFS beamline BL27B at the photon factory of high energy accelerator research organisation KEK (Tsukuba, Japan). At Soleil, the synchrotron operates at 2.75 GeV. The channel-cut crystal Si(111) monochromator was used with an oscillation frequency of 0.5 Hz over 1.1° amplitude in order to gather a complete Au L_3 EXAFS spectrum. Au L_3-edge measurements were conducted in transmission mode using ionisation chambers (Oken) as detectors. At KEK, the synchrotron operates at 2.5 GeV. The beamline utilises a Si(111) double-crystal monochromator. Au L_3-edge measurements were conducted in transmission mode using a gas ionisation detector.

Data analysis was conducted using the Demeter software package.[38] All spectra were initially calibrated to a reference foil sample collected alongside the sample measurement. These were calibrated to 11 919 eV for the Au L_3 edge. The spectra were normalised and background-subtracted by fitting a spline to the pre-edge and post-edge regions. EXAFS data were fitted in Artemis to standards generated by FEFF8.[39] The data was fitted simultaneously to k^1, k^2 and k^3 weighted data across a k-range of 3–12 Å.

Liquid/liquid electrochemistry

Electrochemical measurements were performed using a micro-liquid/liquid interface as reported previously.[40–42] Measurements were performed with either toluene or 1,2-dichloroethane (DCE) as the organic solvent. The supporting electrolyte used in the DCE phase was TOA^+TFPB^- (tetraoctylammonium tetrakis[3,5-bis(trifluoromethyl)phenyl]borate). To examine the heterogeneous Br^- exchange process an aqueous solution containing 0.5 mM $[AuCl_4]^-$, was brought into contact with an organic DCE phase containing x mM TOA^+Br^- (whereby $x = 0$, 0.5, 1, or 2 mM). After phase separation, voltammetry was measured at the interface between a fresh aqueous phase containing 10 mM HCl and the DCE phase. For the homogenous process, TOA^+Br^- and $TOA^+[AuCl_4]^-$ were initially present in the organic DCE phase. The organic electrolyte was added directly before measurement in both cases.

In order to examine the influence of thiol, an aqueous phase containing 10 mM HCl was brought into contact with the toluene phase. The organic phase contained the background electrolyte, bis(triphenylphosphoranylidene)ammonium tetrakis [3,5-bis(trifluoromethyl)phenyl]borate ($BTPPA^+TFPB^-$) along with 0.5 mM $TOA^+[AuCl_4]^-$ or $TOA^+[AuBr_4]^-$ and y mM 1-dodecane thiol (where $y = 0$, 0.2, 0.5, 1, 1.5 or 2 mM). N. B. $BTPPA^+TFPB^-$ was used in the toluene systems due to the solubility of the electrolyte.[36] Voltammetry was performed directly after addition of the supporting electrolyte to the toluene phase in order to avoid the reaction between Au species and $BTPPA^+$. Experiments were performed on an Ivium "Compactstat" (supplied by Alvatek, UK). There was no additional iR compensation.

Nanoparticle synthesis

Tetraoctylammonium salts of $[AuCl_4]^-$ and $[AuBr_4]^-$ were synthesised by mixing equimolar quantities of $Na^+[AuX_4]^-$ and TOA^+X^- in methanol and recrystallising as reported previously.[13,43] In each case, X was either Br or Cl for both salt species. The $TOA^+[AuX_4]^-$ (0.5 mM) species was mixed with 1-dodecane thiol (0, 0.5 or 1.5 mM) in a single organic phase. Following reduction to Au(I), which can be followed by the loss of solution color, BH_4^- (10 mM) was added slowly with stirring. BH_4^- was added either as $NaBH_4$ in an aqueous solution or as $TBA^+BH_4^-$ in DCE (DCE was used as the solubility of $TBA^+BH_4^-$ in toluene was too low).

TEM measurements

Transmission electron micrographs of the nanoparticle samples were collected using a JEM-2100 TEM (JOEL). The nanoparticle solutions were drop-cast onto holey carbon film TEM grids (300 mesh copper grid, Agar Scientific). The particle size distribution analysis was conducted using ImageJ.[44]

Results

Extent of Br^- exchange during $[AuCl_4]^-$ phase transfer

The method developed by Brust and co-workers involves the transfer of $[AuCl_4]^-$, originally present in an aqueous solution, into an adjacent immiscible organic phase.[3] The organic solvent is usually toluene, whilst other solvents have also been shown to work effectively. The Au can be transferred to the organic phase using a phase transfer catalyst by simply shaking the two phases together to drive Au ion exchange. The charge distribution between the two phases is balanced as the more hydrophilic halide ion present in the phase transfer catalyst partitions into the aqueous phase as the Au transfers to the organic (eqn (1), Fig. 1(i)).

$$TOA^+Br^-_{org} + H^+[AuCl_4]^-_{aq} \rightarrow TOA^+[AuCl_4]^-_{org} + H^+Br^-_{aq} \quad (1)$$

The phase transfer catalyst can be either the bromide salt TOA^+Br^- as in the original synthesis, or the chloride salt TOA^+Cl^-. Alternatively, ion exchange can be performed in methanol and the ion-exchanged product recrystallised as $TOA^+[AuCl_4]^-$ or $TOA^+[AuBr_4]^-$.[13,43] If the reaction is performed with $[AuCl_4]^-$ and TOA^+Br^- it results in some exchange of halide ligands on the gold complex (eqn (2), Fig. 1(ii)).

$$xTOA^+Br^-_{org} + TOA^+[AuCl_4]^-_{org} \rightarrow TOA^+[AuCl_{4-x}Br_x]^-_{org} + xTOA^+Cl^-_{org}\ (x = 1\text{–}4) \quad (2)$$

This ligand exchange has been widely reported, although the extent of halide exchange and its significance for the reaction has not been determined. Here, we probe the exchange process by examining the EXAFS response on increasing the TOA^+Br^- : $[AuCl_4]^-$ ratio (Fig. 2, Table 1). The EXAFS response for $[AuCl_4]^-$ and $[AuBr_4]^-$ is similar as they both form a square planar structure. As mentioned in the introduction, however, it is possible to differentiate the two species as there is a significant change in bond length of ~0.15 Å. The data were therefore fit using two scattering paths for each species: the single scattering path Au–X and the linear multi-scattering path Au–X–Au–X–Au. The spectrum of a reference $[AuBr_4]^-$ solution was also fitted in order to obtain the overall amplitude factor S_0^2, which was then fixed at 0.835 for all other fitted spectra.

The fitted EXAFS data show a clear increase in the exchange of Cl^- for Br^- at higher TOA^+Br^- concentrations. This exchange appears to reach a plateau at 4 or 5 equivalents of TOA^+Br^-, with a value that corresponds to an exchange of 3 Cl^- indicating the presence of an average composition $[AuClBr_3]^-$ as the mixed halide species. Indeed, in the original Brust–Schiffrin synthesis 4.44 equivalents of TOA^+Br^- were used, therefore suggesting that $[AuClBr_3]^-$ is the major species present during the reduction process.[3]

Liquid/liquid electrochemistry conducted during the ligand exchange process confirms these results. In this case, measurements were conducted to examine the phase transfer reaction between $[AuCl_4]^-$ in $H^+[AuCl_4]^-_{(aq)}$ and Br^- in $TOA^+Br^-_{(org)}$, as eqn (1), and the ligand exchange reaction between $[AuCl_4]^-$ of $TOA^+[AuCl_4]^-_{(org)}$ and Br^- of $TOA^+Br^-_{(org)}$ as eqn (2). The voltammetric responses indicated that the ligand exchange process can occur in the organic phase (Fig. 3) or as a phase transfer process at a liquid/liquid interface and ligand exchange process (Fig. S1†).

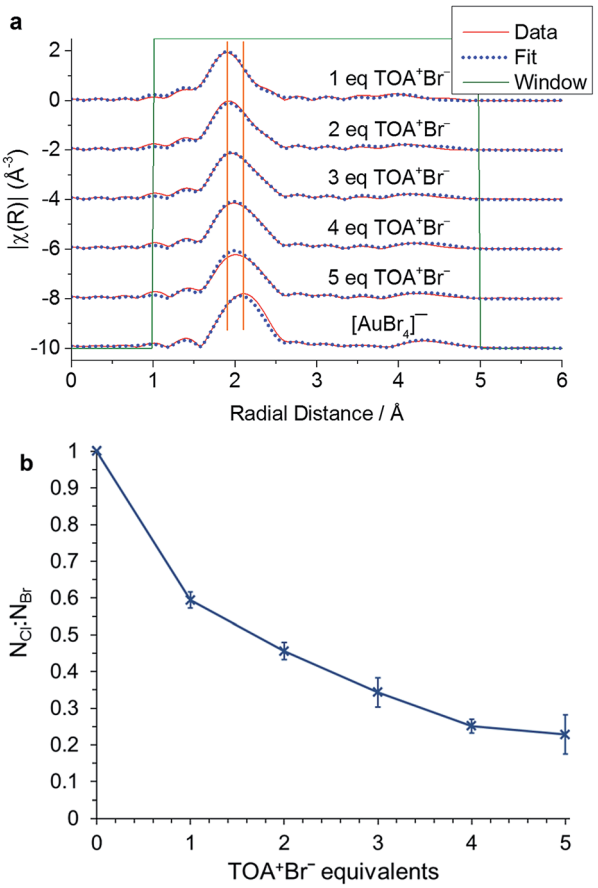

Fig. 2 (a) Fitted EXAFS response following the phase transfer of $[AuCl_4]^-$ by increasing equivalents of TOA^+Br^-. Measurements of the organic phase were performed after mixing 50 mM $HAuCl_4$ in water with 0, 50, 100, 150, 200 or 250 mM TOA^+Br^- in toluene. (b) Variation in Cl^- and Br^- coordination to the gold species on increasing TOA^+Br^- ratio from EXAFS fitting.

Table 1 Fitting parameters for the two species used in Fig. 2[a]

Fitting parameters	$[AuBr_4]^-$	$[AuCl_4]^-$
ΔE_0/eV	2.51 ± 0.43	As for $[AuBr_4]^-$
σ^2/Å^2	0.00256 ± 0.00012	0.00243 ± 0.00027
R/Å	2.41 ± 0.0016	2.26 ± 0.0035

[a] ΔE_0 is the energy shift parameter, σ^2 is the Debye–Waller factor and R is the path length. S_0^2 was fixed at 0.835. The R-factor for the fit was 0.0138.

The formation of $[AuBr_4]^-$ was detected electrochemically as the exchange of Cl^- for Br^- results in the formation of species with different Gibbs energies of ion transfer. The reaction was performed with a range of TOA^+Br^-/Au ratios using either $H^+AuCl_4^-$ as the starting species in the aqueous phase or $TOA^+AuCl_4^-$ in the organic phase. This identifies whether the

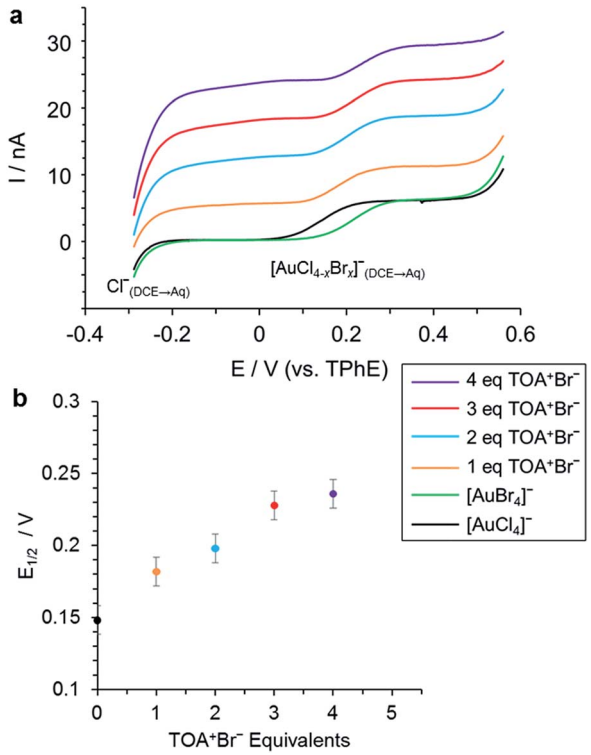

Fig. 3 (a) Voltammetry recorded at the interface between 10 mM HCl in water and 0.2 mM $TOA^+[AuCl_4]^-$ with 0, 0.2, 0.4, 0.6 or 0.8 mM TOA^+Br^- and 1 mM TOATFPB background electrolyte in DCE. 0.2 mM $TOA^+[AuBr_4]^-$ was measured as a reference sample (green line). (b) Shift in half wave potential in the liquid/liquid voltammetry on increasing TOA^+Br^- : Au ratio.

exchange occurs in the bulk phase following transfer, or whether it also occurs across the liquid/liquid interface. Fig. 3 shows the variation in the half wave potential ($E_{1/2}$) for each sample, the voltammetric results are included in Fig. 3 (a). The current wave from −0.3 V corresponds to the transfer of Cl^- from DCE to water, which was formed through the ligand exchange reaction, whilst the 2nd current wave at $E_{1/2}$ approximately 0.15–0.25 V corresponds to the transfer of the anionic Au complex. The position of the latter's half wave potential depends on the degree of halide ligand exchange on the complex. In the presence of TOA^+Br^- (eqn (2)) the $E_{1/2}$ for the 2nd wave shifts to higher values with increasing replacement of Cl by Br ligands. At 4 equivalents of TOA^+Br^-, the $E_{1/2}$ was identical to that of the reference species $[AuBr_4]^-$ (Fig. 3), indicating that ligand exchange of Cl^- for Br^- has reached stoichiometry. The ion transfer potential of $[AuBr_4]^-$ is more positive than that of $[AuCl_4]^-$ due to the increased hydrophilicity of the chloride species. When $[AuCl_4]^-$ was added initially into the aqueous phase, $[AuBr_4]^-$ formation was attained at 5 equivalents of TOA^+Br^- through the phase transfer and ligand exchange reactions (Fig. S1†).

In summary, XAFS has allowed us to characterise the ligand exchange equilibrium in the bulk phase, while voltammetry reveals that the corresponding interfacial process follows approximately the same $[TOA^+Br^-]$ dependence. There are slight differences between the XAFS- and voltammetry-derived compositions, which may stem from the use of different organic solvents for the two experiments and different reactant concentrations.

Single phase reaction of $[AuBr_4]^-$ and thiol

Having confirmed the presence of Br^- in the Au(III) complex following phase transfer, we can now proceed to examine how it influences the reduction protocol. In previous work, we used XAFS to characterise the influence of increasing the 1-dodecane thiol : Au ratio on the reaction with $[AuCl_4]^-$ in a Br free system.[25] Here we use a similar approach based on $[AuBr_4]^-$ as the reaction precursor. First, XAFS was performed on solutions containing a number of different thiol : Au ratios in order to follow the variation in oxidation state and bonding. Speciation in these solutions was then determined using standard spectra for $[AuBr_4]^-$, $[AuBr_2]^-$, and Au(I)SR, to examine the relative concentration of each species. We have previously reported the susceptibility of $[AuCl_2]^-$ to beam induced disproportionation in solution.[45] Therefore to avoid the risk of this process, the $[AuBr_2]^-$ reference spectrum was collected as a solid pellet.

In the case of $[AuCl_4]^-$, the reduction of Au(III) to Au(I) is almost complete at 2 equivalents of thiol. At low thiol concentration (0.5 and 1 eq.) the main product was $[AuCl_2]^-$, while at higher thiol concentrations (2 and 5 eq.) the reaction tended towards Au(I) thiolate formation as the major component.[25] In contrast, when $[AuBr_4]^-$ is used as the reaction precursor there is no evidence for the formation of Au(I) thiolate species, even at high thiol concentrations. Using standards for $[AuBr_4]^-$ and $[AuBr_2]^-$ it can be seen that the majority of the Au(III) has again been reduced to Au(I) at 2 equivalents of thiol (Fig. 4), matching the reaction stoichiometry. Any further excess of thiol causes little variation in the spectral response. Thus in the presence of Br^-, the reaction clearly follows the pathway proposed by Goulet and Lennox, with the reaction leading to the formation of the disulfide species (eqn (3)).[13,28]

$$TOA^+[AuBr_4]^- + 2RSH \rightarrow TOA^+[AuBr_2]^- + RSSR + 2HBr \quad (3)$$

Au(I) thiolate formation has been shown to adversely affect the homogeneity and yield of particles formed in the Brust–Schiffrin synthesis.[13,25] The observation that they are not formed when $[AuBr_4]^-$ is used as the precursor species would indicate that the use of the bromo Au(III) complex should be recommended for the synthesis of gold nanoparticles.

Our observations thus go some way to resolving the discrepancies in the existing literature about Au(I)SR oligomer formation following reduction by alkane thiol. There have been a number of reports on the mechanism of the 2-step synthesis which have shown either the presence[23–25] or absence[13,18] of Au(I) SR formation. We propose that this variability is down to the difference in response for $[AuCl_4]^-$ and $[AuBr_4]^-$ established here. If $[AuCl_4]^-$ is used with TOA^+Cl^- for phase transfer then Au(I)SR formation will occur on addition of thiol. If the original aqueous phase is retained, for either $[AuCl_4]^-$ or $[AuBr_4]^-$,

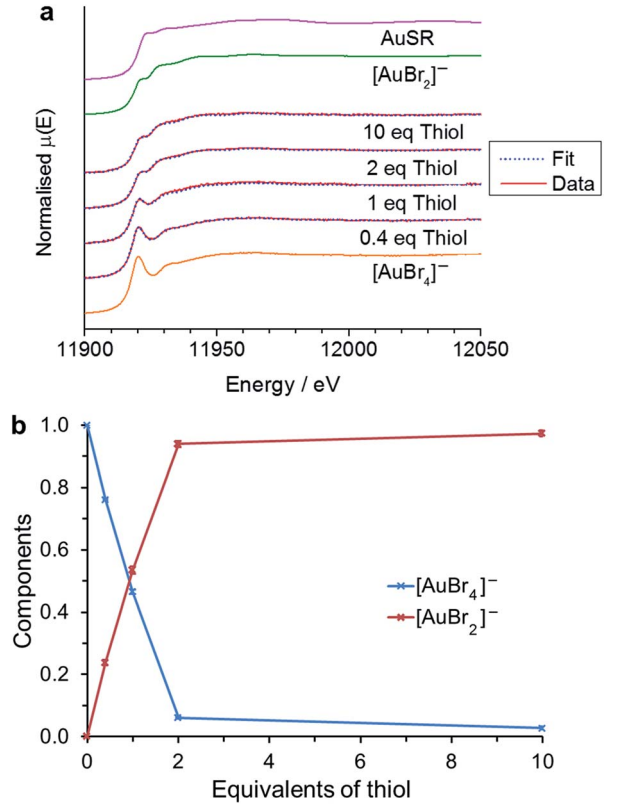

Fig. 4 Variation in XANES response on increasing thiol to $[AuBr_4]^-$ ratio in a single TFT (trifluorotoluene) solution. 5 mM $TOA^+[AuBr_4]^-$ was mixed with 2, 5, 10 or 50 mM thiol (a) data and linear combination fitting to standards for $[AuBr_4]^-$ and $[AuBr_2]^-$. The standard for Au(I)SR is included from ref. 25 (b) the component ratios as a function of thiol equivalents from the linear combination fitting in (a).

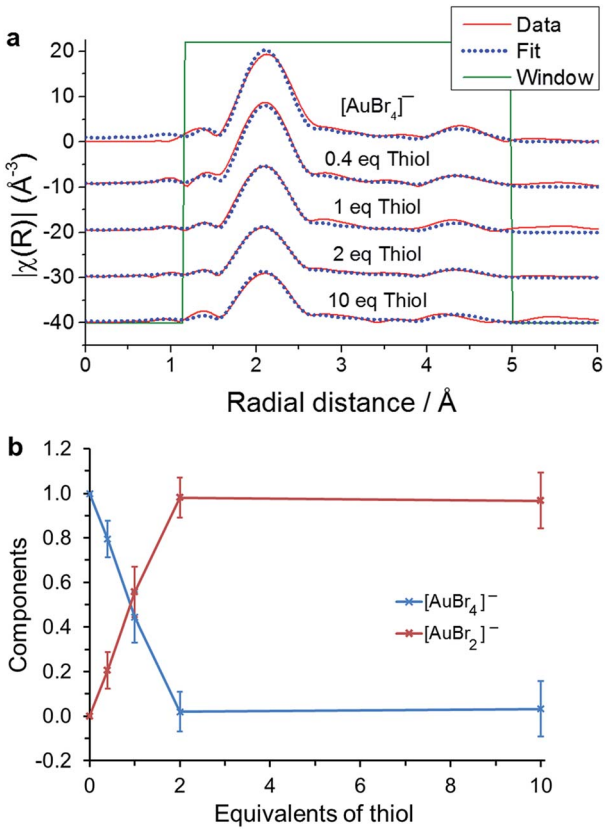

Fig. 5 (a) EXAFS fitting for 5 mM $TOA^+[AuBr_4]^-$ with the additions of 0, 0.4, 1, 2 and 10 equivalents of thiol. (b) Ratio of $[AuBr_4]^-$ to $[AuBr_2]^-$ as a function of thiol concentration.

polymeric Au(I)SR can be observed on reduction by thiol – as the aqueous phase acts as a sink for the HX species formed. The mixed halide species may also form Au(I)SR species at higher thiol : Au ratios in a more polar organic solvent than toluene, such as deuterated chloroform.[24] The difference between Au–S and Au–Br bond lengths allows us to follow the reduction by thiol within the EXAFS, and to determine the formation of intermediate species. As in the EXAFS analysis of the TOA^+Br^- reaction with $[AuCl_4]^-$, the data was considered using the single scattering path Au–Br and the multiple scattering path Au–Br–Au–Br–Au. The data and fits plotted in *R*-space are shown in Fig. 5 with the parameters used in the EXAFS fitting recorded in Table 2.

The fitting model that produced the best agreement with the experimental data suggests, as with the linear combination fitting to the XANES region (Fig. 4), that the only species present are $[AuBr_4]^-$ and $[AuBr_2]^-$. The variation in $[AuBr_4]^-$ and $[AuBr_2]^-$ obtained through EXAFS and XANES analysis agree well, and indicate that there is no significant Au(I) thiol oligomer formation in a single organic phase. However, if the aqueous phase is retained then the white precipitate species characteristic of $(Au(I)SR)_n$ formation can be observed in both cases. The reaction with thiol was also characterised through the use of cyclic voltammetry at a micro-liquid/liquid interface.

Table 2 Fitting parameters for the 2 species used in Fig. 5[a]

Fitting parameters	$[AuBr_4]^-$	$[AuBr_2]^-$
S_0^2	0.896 ± 0.087	As for $[AuBr_4]^-$
ΔE_0/eV	7.72 ± 0.94	As for $[AuBr_4]^-$
σ^2/Å^2	0.00230 ± 0.00056	0.00267 ± 0.00058
R/Å	2.42 ± 0.0025	2.39 ± 0.0049
N	4 (fixed)	2 (fixed)

[a] S_0^2 is the amplitude reduction factor, ΔE_0 is the energy shift parameter, σ^2 is the Debye–Waller factor, R is the bond length and N is the path degeneracy. The *R*-factor for the fit was 0.0270.

Measurements were conducted on samples after 30 minutes and 12 hours of mixing the thiol and $[AuBr_4]^-$ solution. In both cases there was no evidence for Au(I)SR formation (Fig. 6) as there was no current at negative potentials that would correspond to the transfer of Br^- dissociated from $[AuBr_2]^-$ during the formation of $[Au(I)SR]_n$ in toluene as in the reaction ($TOAAuBr_2 + HSR \rightleftarrows Au(I)SR + HBr + TOA^+Br^-$). The formation of $[AuBr_2]^-$ was detected electrochemically at a more negative potential than $[AuBr_4]^-$ transfer due to the reduction by thiol which results in the formation of species with a different Gibbs energy of ion transfer, Fig. 6 (a). The concentration of $[AuBr_4]^-$ and $[AuBr_2]^-$ was determined from the limiting currents in the voltammogram (Fig. 6 (b) and S2†). There is little variation

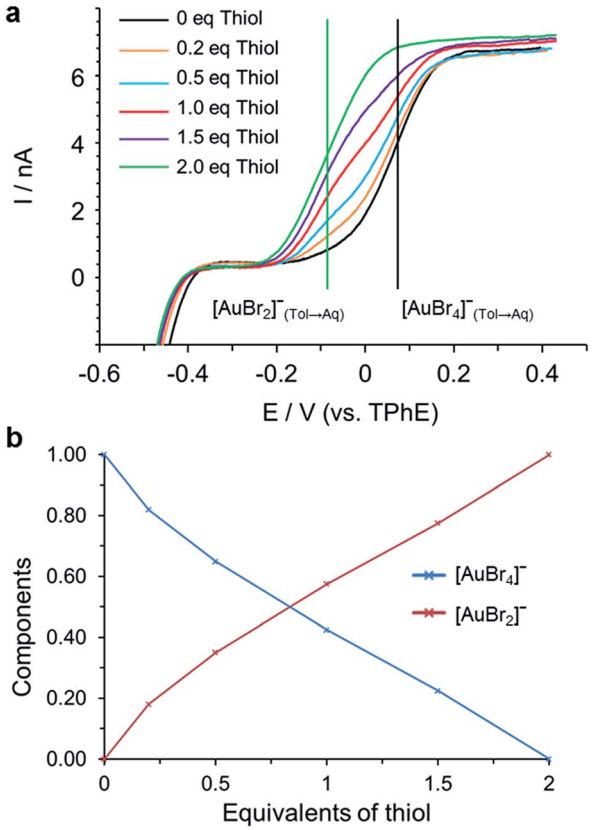

Fig. 6 (a) Voltammetry at a micro-liquid/liquid interface. The toluene phase contained 0.5 mM $TOA^+[AuBr_4]^-$ and 0, 0.2, 0.5, 1, 1.5 or 2 equivalents of thiol, mixed for 12 hours. The electrolytes (10 mM HCl in water and 10 mM BTPPATFPB in toluene) were added directly before the measurements were conducted. (b) Concentration of $[AuBr_4]^-$ and $[AuBr_2]^-$ determined from the limiting current in the voltammogram.

between the two measurements, indicating that the reaction between $[AuBr_4]^-$ and thiol has reached completion after 30 min. This is much more rapid than the interaction between thiol and $[AuCl_4]^-$ examined previously.[25] It was found that $[AuBr_4]^-$ was quantitatively reduced by 2 equivalents of thiol to $[AuBr_2]^-$, which agreed with the results of both the XANES and EXAFS analyses.

Reduction of $[AuBr_2]^-$ by $NaBH_4$

Whilst the only intermediate species formed from $[AuBr_4]^-$ is $[AuBr_2]^-$, the influence that the ratio of thiol to Au has on the properties of the product nanoparticles remains to be examined. The variations between products was therefore characterised at different thiol concentrations by UV-Visible spectroscopy (Fig. 7). $NaBH_4$ solution was brought into contact with toluene containing different thiol : Au ratios, 24 h after mixing. Images of the solutions before and after the reduction are included in the ESI (Fig. S3 and S5†). It is noteworthy that following $NaBH_4$ addition, Au nanoparticles are formed in toluene even in the absence of thiol. Whilst the concentration is lower than for the other samples this is nonetheless a striking observation, as there is no ligand present to stabilise this

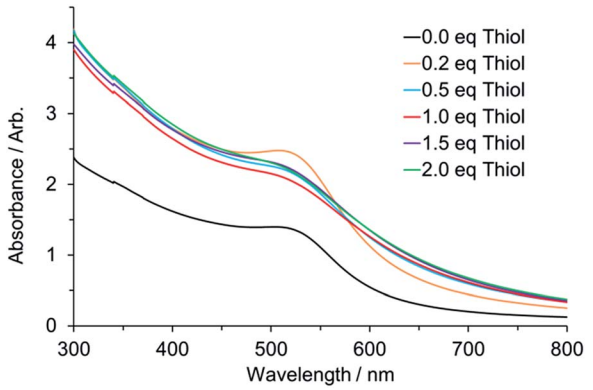

Fig. 7 UV-Vis response for nanoparticles following reduction by BH_4^- formed at different thiol : Au ratios.

suspension by passivating the surface of the particles. TEM of the particles formed in this system are included in Fig. S6.† At present we can only propose that there is some form of electrostatic stabilisation provided by surface adsorption of the Br^- although this is not yet fully understood. The intensity of the SPR peak at ~520 nm matches well with the variation in nanoparticle size on increasing thiol concentration that was reported previously.[26]

Control over nanoparticle shape and size

The proposed improvements in the synthetic protocol have been examined through TEM and UV-Vis analysis of the reaction products. As reported by Haiss *et al.*[46] UV-Vis does not give an accurate measure of nanoparticle size for particles below ~5 nm, so size distribution information was obtained using TEM. The reduction of $[AuCl_4]^-$ and $[AuBr_4]^-$ was carried out using 1 : 1 and 3 : 1 eq. thiol : Au. Following reduction by thiol, BH_4^- was added either in the form of aqueous $NaBH_4$ or as $TBA^+BH_4^-$ in DCE. Fig. 8 shows the results for $[AuCl_4]^-$ and $[AuBr_4]^-$ reduction by $TBA^+BH_4^-$. As can be seen, $[AuBr_4]^-$ results in a slightly larger deposition product 3.0 nm instead of 2.0 nm which is similar to previously reported data.[15] We suggest that the smaller size of nanoparticles in the Cl system

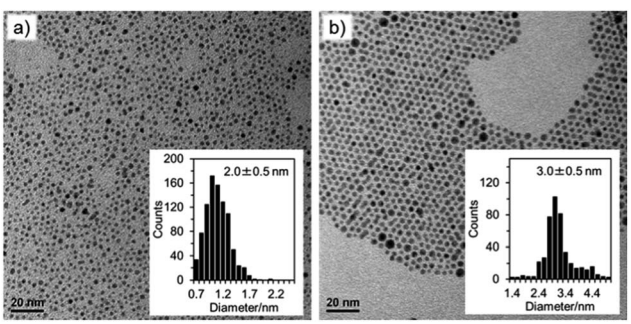

Fig. 8 TEM micrographs of the reduction products using (a) $[AuCl_4]^-$ and (b) $[AuBr_4]^-$. 0.5 mM TOA^+ Au salt was mixed with 1.5 mM 1-dodecane thiol in toluene and contacted with a solution containing 20 mM $TBA^+BH_4^-$ in DCE.

relates to the presence of Au(I)SR species prior to the addition of BH_4^- which enables more rapid passivation of the nanoparticles during growth.

Whilst the standard deviation in particle diameter is the same for both species, it can be seen from the histogram that there is a more uniform distribution for the $[AuBr_4]^-$ nanoparticles than for the $[AuCl_4]^-$ particles. The UV-Vis response also indicates a higher concentration of nanoparticles when the bromoaurate precursor species is used (Fig. S8†). Fig. S6† shows the TEM micrographs for the formation of nanoparticles at 0 eq. thiol, at a 1 : 1 ratio and through reduction by $NaBH_4$.

Conclusions

The significant influence of Br^- on the Brust–Schiffrin synthesis of gold nanoparticles has been examined quantitatively. The possible reaction pathways are provided in Fig. 1 and S8† for the presence and absence of Br^-, respectively. We have verified that the use of TOA^+Br^- as the phase transfer catalyst results in the formation of a mixed halide gold complex through exchange of Br^- for Cl^- ligands. In the Brust–Schiffrin protocol a 5-fold excess, or greater, of TOA^+Br^- over the Au precursor was necessary to obtain a high yield of nanoparticles. 1 equivalent of TOA^+Br^- is required in order to transfer $[AuCl_4]^-$ from the aqueous phase to the organic. Subsequently, 4 equivalents of TOA^+Br^- are consumed through halide exchange from $[AuCl_4]^-$ to $[AuBr_4]^-$. The $[AuBr_4]^-$ is reduced to $[AuBr_2]^-$, which is fairly stable even at high thiol concentration, whereas $[AuCl_2]^-$ species have a propensity to form a white precipitate of Au(I)SR at high thiol concentration, which tends to oligomerise. The insoluble Au(I) thiolate species is not readily reduced by $NaBH_4$. When $[AuBr_4]^-$ is used as the Au precursor then there is no formation of Au(I)SR species in toluene, TFT or DCE, which may be related to the higher thermodynamic stability (as reflected in a lower reduction potential) of the gold bromides, compared to gold chlorides. We note that $K[AuBr_4]$ is not classified as an irritant, unlike $K[AuCl_4]$, which implies more convenient handling of the synthesis in the laboratory. The use of $[AuBr_4]^-$ also ensures that TOA^+Br^- is only used during the phase transfer process. Electrochemical measurements indicated that the reduction of Au(III) complexes with higher bromo ligand content proceeds more rapidly than for the chloro complexes. If the aqueous phase is retained then polymeric Au(I) thiolate species are observed in all cases. As Au(I) thiolate formation can be fully avoided, the yield of metal nanoparticles in the synthesis can be increased. We propose that the synthetic procedure utilising $TOA^+[AuBr_4]^-$ as the gold precursor and addition of an organic solution of BH_4^- will result in the most robust synthetic protocol.

Conflicts of interest

There are no conflicts to declare.

Acknowledgements

The authors wish to acknowledge the award of beamtime on the ROCK beamline at Synchrotron SOLEIL under proposal number 20151221. The work on ROCK was supported by a public grant overseen by the French National Research Agency (ANR) as part of the 'Investissements d'Avenir' program (reference: ANR-10-EQPX-45). The authors also acknowledge the award of beamtime at KEK (2015G026). SLMS and RAWD acknowledge the financial support from the EPSRC through an EPSRC-NSF Materials World Network grant EP/H047786/1 and RAWD acknowledges further support from grant EP/K007033/1 which has contributed to this research. AU wishes to acknowledge grant (No. 16K06958) from the Ministry of Education, Culture, Sports, Science and Technology, Japan. Original EXAFS data files are available at Mendeley.com.

References

1 J. Turkevich, P. C. Stevenson and J. Hillier, *Discuss. Faraday Soc.*, 1951, 55–75.
2 G. Frens, *Nat. Phys. Sci.*, 1973, **241**, 20–22.
3 M. Brust, M. Walker, D. Bethell, D. J. Schiffrin and R. Whyman, *J. Chem. Soc., Chem. Commun.*, 1994, 801–802.
4 M. Brust, J. Fink, D. Bethell, D. J. Schiffrin and C. Kiely, *J. Chem. Soc., Chem. Commun.*, 1995, 1655–1656.
5 P. X. Zhao, N. Li and D. Astruc, *Coord. Chem. Rev.*, 2013, **257**, 638–665.
6 S. Murthy, T. P. Bigioni, Z. L. Wang, J. T. Khoury and R. L. Whetten, *Mater. Lett.*, 1997, **30**, 321–325.
7 S. Y. Kang and K. Kim, *Langmuir*, 1998, **14**, 226–230.
8 S. W. Chen and J. M. Sommers, *J. Phys. Chem. B*, 2001, **105**, 8816–8820.
9 S. W. Chen, K. Huang and J. A. Stearns, *Chem. Mater.*, 2000, **12**, 540–547.
10 G. Corthey, A. A. Rubert, A. L. Picone, G. Casillas, L. J. Giovanetti, J. M. Ramallo-Lopez, E. Zelaya, G. A. Benitez, F. G. Requejo, M. Jose-Yacaman, R. C. Salvarezza and M. H. Fonticelli, *J. Phys. Chem. C*, 2012, **116**, 9830–9837.
11 O. Toikkanen, V. Ruiz, G. Ronholm, N. Kalkkinen, P. Liljeroth and B. M. Quinn, *J. Am. Chem. Soc.*, 2008, **130**, 11049–11055.
12 E. E. Foos, A. W. Snow, M. E. Twigg and M. G. Ancona, *Chem. Mater.*, 2002, **14**, 2401–2408.
13 P. J. G. Goulet and R. B. Lennox, *J. Am. Chem. Soc.*, 2010, **132**, 9582–9584.
14 S. R. K. Perala and S. Kumar, *Langmuir*, 2013, **29**, 14756–14762.
15 T. R. Graham, R. Renslow, N. Govind and S. R. Saunders, *J. Phys. Chem. C*, 2016, **120**, 19837–19847.
16 Y. Li, O. Zaluzhna and Y. Y. J. Tong, *Langmuir*, 2011, **27**, 7366–7370.
17 Y. Li, O. Zaluzhna and Y. Y. J. Tong, *Chem. Commun.*, 2011, **47**, 6033–6035.
18 Y. Li, O. Zaluzhna, B. L. Xu, Y. A. Gao, J. M. Modest and Y. J. Tong, *J. Am. Chem. Soc.*, 2011, **133**, 2092–2095.
19 Y. Li, O. Zaluzhna, C. D. Zangmeister, T. C. Allison and Y. Y. J. Tong, *J. Am. Chem. Soc.*, 2012, **134**, 1990–1992.
20 O. Zaluzhna, Y. Li, T. C. Allison and Y. Y. J. Tong, *J. Am. Chem. Soc.*, 2012, **134**, 17991–17996.

21 O. Zaluzhna, Y. Li, C. Zangmeister, T. C. Allison and Y. J. Tong, *Chem. Commun.*, 2012, **48**, 362–364.
22 M. J. Hostetler, J. E. Wingate, C. J. Zhong, J. E. Harris, R. W. Vachet, M. R. Clark, J. D. Londono, S. J. Green, J. J. Stokes, G. D. Wignall, G. L. Glish, M. D. Porter, N. D. Evans and R. W. Murray, *Langmuir*, 1998, **14**, 17–30.
23 L. L. Zhu, C. Zhang, C. C. Guo, X. L. Wang, P. C. Sun, D. S. Zhou, W. Chen and G. Xue, *J. Phys. Chem. C*, 2013, **117**, 11399–11404.
24 C. H. Yu, L. L. Zhu, R. C. Zhang, X. L. Wang, C. C. Guo, P. C. Sun and G. Xue, *J. Phys. Chem. C*, 2014, **118**, 10434–10440.
25 A. Uehara, S. G. Booth, S. Y. Chang, S. L. M. Schroeder, T. Imai, T. Hashimoto, J. F. W. Mosselmans and R. A. W. Dryfe, *J. Am. Chem. Soc.*, 2015, **137**, 15135–15144.
26 S. R. K. Perala and S. Kumar, *Langmuir*, 2013, **29**, 9863–9873.
27 M. K. Corbierre and R. B. Lennox, *Chem. Mater.*, 2005, **17**, 5691–5696.
28 B. M. Barngrover and C. M. Aikens, *J. Am. Chem. Soc.*, 2012, **134**, 12590–12595.
29 Y. Y. Huang, T. Yao, Z. H. Sun and S. Q. Wei, *J. Phys.: Conf. Ser.*, 2013, **430**(1), 012033.
30 Y. F. Cheng and D. J. Schiffrin, *J. Chem. Soc., Faraday Trans.*, 1996, **92**, 3865–3871.
31 C. Johans, R. Lahtinen, K. Kontturi and D. J. Schiffrin, *J. Electroanal. Chem.*, 2000, **488**, 99–109.
32 C. Johans, J. Clohessy, S. Fantini, K. Kontturi and V. J. Cunnane, *Electrochem. Commun.*, 2002, **4**, 227–230.
33 A. Trojanek, J. Langmaier and Z. Samec, *J. Electroanal. Chem.*, 2007, **599**, 160–166.
34 A. Uehara, T. Hashimoto and R. A. W. Dryfe, *Electrochim. Acta*, 2014, **118**, 26–32.
35 S. G. Booth, A. Uehara, S. Y. Chang, J. F. W. Mosselmans, S. L. M. Schroeder and R. A. W. Dryfe, *J. Phys. Chem. C*, 2015, **119**, 16785–16792.
36 M. Kasuno, Y. Matsuyama and M. Iijima, *ChemElectroChem*, 2016, **3**, 694–697.
37 V. Briois, C. La Fontaine, S. Belin, L. Barthe, T. Moreno, V. Pinty, A. Carcy, R. Girardot and E. Fonda, *J. Phys.: Conf. Ser.*, 2016, **712**, 012149.
38 B. Ravel and M. Newville, *J. Synchrotron Radiat.*, 2005, **12**, 537–541.
39 A. L. Ankudinov and J. J. Rehr, *Phys. Rev. B*, 1997, **56**, R1712–R1715.
40 G. Taylor and H. H. J. Girault, *J. Electroanal. Chem.*, 1986, **208**, 179–183.
41 M. C. Osborne, Y. Shao, C. M. Pereira and H. H. Girault, *J. Electroanal. Chem.*, 1994, **364**, 155–161.
42 H. Ohde, A. Uehara, Y. Yoshida, K. Maeda and S. Kihara, *J. Electroanal. Chem.*, 2001, **496**, 110–117.
43 P. Braunstein and R. J. H. Clark, *J. Chem. Soc., Dalton Trans.*, 1973, 1845–1848.
44 C. A. Schneider, W. S. Rasband and K. W. Eliceiri, *Nat. Methods*, 2012, **9**, 671–675.
45 S. Y. Chang, A. Uehara, S. G. Booth, K. Ignatyev, J. F. W. Mosselmans, R. A. W. Dryfe and S. L. M. Schroeder, *RSC Adv.*, 2015, **5**, 6912–6918.
46 W. Haiss, N. T. K. Thanh, J. Aveyard and D. G. Fernig, *Anal. Chem.*, 2007, **79**, 4215–4221.